Mechanistic modeling of fingering, nonmonotonicity, fragmentation, and pulsation within gravity/buoyant destabilized two-phase/unsaturated flow

Robert J. Glass and Lane Yarrington

Flow Visualization and Processes Laboratory, Sandia National Laboratories, Albuquerque, New Mexico, USA

[1]   Fingering, nonmonotonicity, fragmentation, and pulsation within gravity/buoyant destabilized two-phase/unsaturated flow systems has been widely observed with examples in homogeneous to heterogeneous porous media, in single fractures to fracture networks, and for both wetting and nonwetting invasion. To model this phenomena, we consider a mechanistic approach based on forms of modified invasion percolation (MIP) that include gravity, the influence of the local interfacial curvature along the phase-phase interface, and the simultaneous invasion and reinvasion of both wetting and nonwetting fluids. We present example simulations and compare them to experimental data for three very different situations: (1) downward gravity-driven fingering of water into a dry, homogeneous, water-wettable, porous medium; (2) upward buoyancy-driven migration of gas within a water saturated, heterogeneous, water-wettable, porous medium; and (3) downward gravity-driven fingering of water into a dry, water-wettable, rough-walled fracture.   *INDEX TERMS:* 1829 Hydrology: Groundwater hydrology; 1875 Hydrology: Unsaturated zone; 1832 Hydrology: Groundwater transport; *KEYWORDS:* instability, fingering, modified invasion percolation, preferential flow, fractures, pulsation

1.   Introduction

[2]   The displacement of one fluid by another within a porous media has been studied extensively in the past 50 years due to its relevance in applied problems ranging from the design of manufacturing processes, to fossil energy extraction, to water and contaminant transport within the subsurface. In context of subsurface water resources, immiscible fluids such as air, water, oils, or solvents, often have different densities and viscosities and can, on occasion, form fingers when displaced due to viscous or density instability. With regard to environmental problems, the density instability is of greatest importance with a variety of examples that cover both the unsaturated and saturated zones. The gravity-driven fingering of water downward into water-wettable, unsaturated media has been studied extensively since the early 1970s [e.g., *Hill and Parlange*, 1972]. Below the water table, the fingering of dense nonaqueous phase liquids (DNAPLs) downward into water-wettable, saturated media has been studied since the 1980s [e.g., *Schwille*, 1988]. Interestingly, a number of studies over the past decade have discovered that under such destabilized displacement conditions the phase saturation field can undergo decreases in saturation or "nonmonotonicity" and occasionally fragment and pulsate, even under conditions of constant applied flux.

[3]   During low flow gravity-driven fingering of water into water-wettable, unsaturated porous media, finger tips are found to nearly saturate and then drain a distance behind, thus creating a nonmonotonic profile along the length of the finger [*Glass et al.*, 1989a; *Selker et al.*, 1992]. In these situations, a nearly saturated finger tip forms and then drains a distance behind as the tip passes. Water continues to flow down the desaturated finger core to supply the finger tip from the source above. A slightly different behavior is found when a nonwetting fluid forms a gravity-driven finger in porous media. Here, the finger is no longer macroscopic but "pore scale" consisting of a series of irregular ganglia connected by single pores [*Schwille*, 1988]. As with the wetting finger, the nonwetting finger also desaturates a distance behind the finger tip under constant low flow conditions. However, on desaturation, the nonwetting phase fragments into disconnected ganglia distributed along the length of the finger [*Meakin et al.*, 1993]. Under conditions of constant supply, the nonwetting phase continues to flow down the finger as pulses that intermittently connect the ganglia and replenish the advancing finger tip.

[4]   A similar behavior is found in fractures where macroscopic fingers form for wetting invasion and aperture-correlation-scale fingers form for nonwetting. However, in fractures we find that flow structure can exhibit fragmentation and pulsation behind the finger tip for both wetting and nonwetting fluids [*Nicholl et al.*, 1993; *Su et al.*, 1999, 2001]. Interestingly, in the context of nonwetting buoyant/gravity-driven migration in heterogeneous sands, pulsation has also been documented to occur at the unit scale where

pools of the nonwetting phase behind heterogeneity induced capillary barriers "throb," their heights increasing and decreasing in time [*Glass et al.*, 2000a].

[5] At present, we do not know the full extent to which fingering and associated phenomena (nonmonotonicity, fragmentation, pulsation) occur within nature. However, based on current understanding, we can surmise that the critical parameter space will be defined by at least: local porous media and/or fracture topology (pore size distribution, connectivity and spatial correlation; aperture field distribution and spatial correlation); larger scale heterogeneity (property juxtaposition, magnitude of property mismatch, length scales); wetting properties (static and dynamic contact angles, media microroughness); fluid properties (interfacial tension, density, viscosity); and boundary/ initial conditions (flow rates, initial fluid saturations and distributions). As an example, for gravity-driven fingering of a wetting fluid in porous media, experiments conducted by a number of researchers suggest that media nonlinearity (pore size distribution) and media heterogeneity as well as the applied flux and initial saturation of the wetting fluid all play a role in defining occurrence [*Glass and Nicholl*, 1996]. However, the transition from fingering where nonmonotonicity creates a hysteretically heterogeneous media and controls subsequent transport, to diffusive behavior where the standard porous continuum representation of the physics embodied in the Richards equation applies, is not known.

[6] While analysis of such phenomena must be considered with a range of approaches, mechanistic models that can incorporate small scale physics and allow parametric studies are necessary. In this paper we consider a mechanistic model based on forms of modified invasion percolation (MIP) for application in context of both porous media and fractures. Such models have been successful in a range of situations through "modifications" of the original invasion percolation (IP) process (section 2.). For our application, we employ modifications that include gravity and model capillary forces along the growing interface through calculation of the local interface geometry (see section 2.1 for porous media and section 2.2 for fractures). To model nonmonotonicity and fragmentation, we include further modifications to allow the simultaneous invasion of the invading phase as well as the reinvasion of the defending phase as a displacement progresses (see section 2.3). As both an illustration and an assessment of the MIP model, we apply and compare model results to three very different gravity/buoyancy-driven situations where published experimental data exists (section 3.). First, we consider the downward gravity-driven fingering of water into a dry, homogeneous, water-wettable, porous medium (section 3.1). We then focus on the upward buoyancy-driven migration of gas within a water saturated, heterogeneous, water-wettable, porous medium (section 3.2). Finally, we turn our attention to fractures and consider the downward gravity-driven fingering of water into a vertical, dry, water-wettable, rough-walled fracture (section 3.3). In each case we find the mechanistic MIP model can reproduce many qualitative and quantitative aspects found in the experiments. Because the temporal dynamics of fragmentation and pulsation is difficult to convey in our "still" figures and measurements, we also present anima-tions of the experiments and simulations and encourage the reader to view them. These animations are available at http://agu.org/journals/wr/.

2. Model Formulation

[7] Invasion percolation (IP) models phase invasion on a network where the pressure within each phase varies as a function of time but not in space [*Wilkinson and Willemsen*, 1983]. This is a reasonable assumption in the limit of infinitesimal flow rate (quasi-static) where viscous forces are negligible with respect to capillary forces (i.e., small capillary number). IP is implemented with a given network connectivity, each pore, or more generally a "node", having an assigned invasion pressure. Selected nodes are filled with the invading phase to form a boundary surface or source, and all others connected to this source are made available for further invasion; the one with the lowest invasion pressure is found and invaded. This event modifies the list of nodes connected to the invading phase, which is once again sorted to find and invade the site with the lowest pressure, and so on. If the defending phase is incompressible, then nodes that become surrounded by the invader (entrapped) are removed from the list. Conversely, if the defender fluid is infinitely compressible or will dissolve in the invading phase, then entrapped nodes are not removed. Invasion continues until a specified pressure cutoff or spatial extent is achieved.

[8] In recent years, IP has been successfully modified (MIP) for a variety of situations to better reflect the underlying physics of the invasion process. Gravity can be included as a simple gradient within IP to yield fingers [*Glass and Yarrington*, 1989, 1996; *Meakin et al.*, 1992] that conform well to experiments in granular porous media for nonwetting invasion [*Meakin et al.*, 1992]. For this situation, a pore scale finger is produced, its width dependent on the pore size distribution [*Glass and Yarrington*, 1996]. However for wetting invasion, experiments show macroscopic fronts that yield macroscopic fingers of well defined width. Considering the fluid-fluid geometry within a pore under wetting invasion, one finds that when a pore is fed by multiple necks, a multiple-adjacent-neck-pore-filling "facilitation" occurs. Because the pressure to invade a given pore is dependent on the local interfacial geometry within the pore, having more than one neck feed a pore changes this geometry and "facilitates" its filling by lowering the required invasion pressure. When such a modification is included, MIP can simulate the macroscopic nature of wetting invasion both in the absence of gravity [*Blunt and Scher*, 1995] and in its presence where simulated finger widths overlap those found experimentally [*Glass and Yarrington*, 1989, 1996]. We note that, as found for the nonwetting case, wetting finger width is also dependent on pore size distribution. With regard to rough-walled fractures, a similar modification for local interface geometry has been found to be important in yielding macroscopic gravity-driven fingers in vertical fractures [*Glass*, 1993] as well as macroscopic phase entrapment in horizontal fractures [*Glass et al.*, 1998; *Hughes and Blunt*, 2001]. We note in passing that many other forms of MIP have been proposed to accommodate a variety of additional processes including gas diffusion during drying [*Prat*, 1993] and film flow

during wetting [*Blunt and Scher*, 1995], as well as the inclusion of viscous forces [*Xu et al.*, 1998; *Ewing and Berkowitz*, 1998; *Glass et al.*, 2001]. Additionally, forms of MIP have been upscaled to model phase displacements within heterogeneous aquifers under gravity destabilized [*Glass et al.*, 1995] and gravity-stabilized situations [*Kueper and McWhorter*, 1992; *Ioannidis et al.*, 1996].

[9] While the modifications to IP for the local geometry at the phase-phase interface allow us to simulate accurate finger widths in both porous media and fractures, such fingers are static. Thus they do not desaturate behind the finger tip as we find for wetting fingers in porous media, nor do they fragment or pulse as we find for nonwetting fingers in porous media and wetting and nonwetting fingers in fractures. A full mechanistic model for gravity/buoyant destabilized displacements must simulate this behavior as well. Modifications that allow phase fragmentation to occur have been incorporated into both IP and IP with gravity for nonwetting invasion [*Meakin et al.*, 1993; *Wagner et al.*, 1997; *Auradou et al.*, 1999; *Amundsen et al.*, 1999]. However, without the influence of local geometry of the phase-phase interface, fragmentation dominates the invasion process where for many cases in nature it does not occur.

[10] Here we are interested in modeling gravity/buoyant destabilized displacements at the quasi-static limit (low flow, small capillary number) in both porous media and rough-walled fractures. We are also interested in the invasion of both the wetting fluid such as we find in gravity-driven fingering in unsaturated or vadose zone environments, and the nonwetting fluid as we find below the water table for most DNAPL migration situations. Thus we formulate our mechanistic model to include gravity, the influence of local geometry of the phase-phase interface, and the simultaneous invasion and reinvasion of wetting and nonwetting fluids. We make use of the near-pore-scale macro-MIP (NP-MMIP) approach for porous media recently presented by *Glass et al.* [2001] and incorporate facilitation for wetting invasion (section 2.1). For fractures we extend the model of *Glass et al.* [1998] that incorporates both aperture induced and in the plane of the fracture or "in-plane" interfacial curvature to also include gravity (section 2.2). For both porous media and fracture models we then incorporate the simultaneous invasion and reinvasion of both wetting and nonwetting phases within the network along with hysteresis appropriate to each (section 2.3).

2.1. Porous Media

[11] In the work of *Glass et al.* [2001], a form of "macro" modified invasion percolation (MMIP) was conceptualized at the near pore (NP) scale. This approach allows us to model pore scale behavior without the explicit consideration of individual necks and pores. NP blocks that reflect the behavior of an underlying small scale network replace the "ball and stick" conceptualization. Each NP block has its own threshold entry pressure for wetting or nonwetting invasion as determined for the material of interest using standard wetting and drainage pressure-saturation measurements. We now simply consider each block to have two threshold R values, one specific for wetting and the other for nonwetting invasion. Additionally, for wetting invasion we consider facilitation as introduced by *Glass and Yarrington* [1989, 1996] and *Blunt and Scher* [1995].

[12] The capillary pressure required to span the block is given by

$$P_c = \frac{-2\sigma \cos(\alpha)}{R_i} \tag{1}$$

where σ is the interfacial tension, and α is the effective contact angle within the fluid/fluid/solid system (α between 0 and 90 degrees for wetting and 90 and 180 for nonwetting invasion). R_i is the local threshold radius for wetting (R_w), or drainage (R_d), respectively. Conceptually, R_w and R_d represent the critical curvatures that must be achieved to span or "percolate" a given block.

[13] Gravity forces are represented by the hydrostatic pressure:

$$P_g = \Delta_{\rho g z} \tag{2}$$

where $\Delta\rho$ is the density difference between the two fluids ($\rho_{defender}$-$\rho_{invader}$), z is the distance into the network, and g is the component of the acceleration due to gravity in the direction of z. The total invasion pressure for a block is simply given by

$$P_t = \frac{-2\sigma \cos(\alpha)}{R_i} + \Delta\rho g z \tag{3}$$

[14] For wetting entry of a block we model facilitation by adjusting R_w to a facilitated value R_{wf} by

$$R_{wf} = R_w \left(2 - \left(\frac{\frac{n}{n_f} - \frac{1}{n_f}}{1 - \frac{1}{n_f}} \right) \right) \tag{4}$$

where n is the number of adjacent blocks that contain the wetting phase and n_f is the number of blocks at which the effect no longer contributes. Thus R_w is increased from its assigned value by a factor of two when a single block is connected and is incrementally reduced until it reaches the fully facilitated value when n reaches n_f. Idealized two dimensional geometries were considered by *Glass and Yarrington* [1989, 1995] to yield n_f equal to half the connectivity. *Blunt and Scher* [1995] used a similar relationship with n_f equal to a half. We adopt this value as general in our work presented here. We note that implementation of facilitation requires that we recalculate P_t for those blocks affected at the end of each growth step.

2.2. Fractures

[15] MIP for fractures was presented by *Glass et al.* [1998]. There the fracture aperture field was conceptualized as a planar checkerboard of individual elements with a four-fold connectivity, the center of each element with a known local aperture. The aperture invasion pressure, P_c, is a function of the two principal radii of interfacial curvature, r_1 and r_2, and the surface tension, σ, as given by the Laplace relation:

$$P_c = -\sigma \left(\frac{1}{r_1} + \frac{1}{r_2} \right) \tag{5}$$

where one principal radius of curvature, r_1, is normal to the plane of the fracture and the other, r_2, is in-the-plane of the

fracture. r_1 intersects the fracture walls while that defined by r_2 does not. Therefore wettability affects only r_1. r_1 is related geometrically to the local aperture (a) and local convergence/divergence angle of the fracture surfaces (β) through the local contact angle (α) at the fluid/fluid/fracture surface:

$$r_1 = \frac{a}{2\cos(\alpha + \beta)} \qquad (6)$$

The convergence/divergence angle of the two fracture surfaces, β, is defined as positive for widening aperture and negative for narrowing.

[16] Here r_2 is modeled as a function of the included angle, γ, between two vectors representing the average interface once an aperture is invaded:

$$r_2 = \langle r_2 \rangle \tan\left(\frac{\gamma}{2}\right) \qquad (7)$$

where $\langle r_2 \rangle$ is a representative r_2 for the aperture field. γ is defined looking from the invading fluid (see corrected figure in the work by *Glass et al.* [2000b]). To avoid dependence on the aperture field discretization resolution, $\langle r_2 \rangle$ and the calculation of γ are linked to the spatial structure of the aperture field. For spatially correlated fields, the random field's correlation length, λ, is taken as its characteristic length scale ($\langle r_2 \rangle \sim 0.5\,\lambda$) and γ is determined as an average of unit vectors extending from the subject aperture to each neighboring aperture location along the interface within a distance λ.

[17] Incorporating gravity forces as defined in (2) and these definitions for r_1 and r_2, we write for P_t:

$$P_t = -2\sigma\left(\frac{\cos(\alpha + \beta)}{a} - \frac{1}{\lambda \tan(\gamma/2)}\right) + \Delta\rho g z \qquad (8)$$

Implementation of in-plane curvature requires that P_t be recalculated after each growth step both for all neighboring apertures along the interface within the distance λ and for nearest neighbors where the directionality of β must be incorporated. We emphasize that application of this algorithm requires a discretization of the aperture field tied to its correlation length (i.e., at least ~ 5 grid blocks per correlation length).

2.3. Simultaneous Invasion and Reinvasion

[18] To allow fingers to desaturate behind their tips as well as fragment and pulsate, we must allow the simultaneous invasion and reinvasion of the wetting and nonwetting fluids. In the following, we continue to consider the invading process from the perspective of the global invading phase with P_t to invade a site given as above for the invading phase. We now define the pressure for a site filled with the invading fluid to "vacate" as given by the pressure to reinvade a site with the defending fluid. For the porous media model, we simply take $R_w = 2R_d$ for the site as a reasonable representation of geometric hysteresis and include facilitation if the global invading phase is nonwetting. For the fracture, we simply calculate the in-plane curvature to vacate the site. For both the porous media and fracture, the contact angle can be changed from the invasion value to a different vacating value such as to include contact angle hysteresis if so desired. It should be noted that with

and without simultaneous invasion and reinvasion, the maximum extent of the invading phase structures are identical at breakthrough except on rare occasions where round-off error during the calculation of in-plane curvature for fractures can create alternative paths.

[19] At the quasi-static limit, a site in either model will only vacate if the following condition is met:

$$P_{cVac} = P_{cFill} - P_g \qquad (9)$$

where P_{cFill} is given by the most recently invaded site within a given connected cluster and P_g is calculated using the distance between the site in question and the furthest penetration into the network within the connected cluster. Percolation proceeds as follows: (1) available sites for filling are sorted and the lowest pressure site is filled; (2) available sites for vacating are sorted and the highest pressure site is tested, if it meets the criterion, then it is vacated; (3) pressures for potential filling and vacating sites are recalculated based on changes in adjacency for facilitation and for in-plane curvature; then (4) repeat.

[20] As the process proceeds, three types of clusters evolve. The first type is connected to the source. As a simulation begins, all clusters are of this type and for a single source we have a single connected cluster. When the cluster fragments, the daughter clusters continue to move independently (second type, disconnected) as long as the condition (9) is met for the cluster. When (9) is not satisfied, the cluster becomes stagnant and stops moving (third type, stagnant). As invasion progresses, a large number of clusters evolve. We "service" each of the moving clusters independently with a single fill/vacate cycle in order from the furthest into the network back to the source. The cluster connected to the source is serviced at a rate that can be specified as different from the disconnected moving daughters. A lower rate simulates a lower supply rate to the system and allows the disconnected clusters to move as far as possible on their own before they become reconnected to new invading phase from the source.

[21] Finally we note that, on occasion, situations arise where, as we approach the criterion (9) within a disconnected cluster, the same sites repeatedly fill and vacate, the growth process becoming captured in a "vibration" cycle where the cluster no longer moves. When this occurs, the global growth process is slowed as vibrating clusters must be serviced at each step. We implemented a series of algorithms to detect cyclic capture and, once detected, we stagnate the cluster. If detection fails, growth is slowed until the source cluster eventually spawns new independently moving daughters which remove the vibration on contact.

3. Example Simulations and Comparison to Experiment

[22] We illustrate and assess the behavior of the MIP model for three situations reported in the literature where fingering, nonmonotonicity, fragmentation, and pulsation have been documented under conditions of gravity/buoyant destabilization with negligible viscous influence. In porous media, we first consider macroscopic gravity-driven wetting fingers and their nonmonotonic profile in homogeneous sands as discovered by *Glass et al.* [1989a]. For a non-
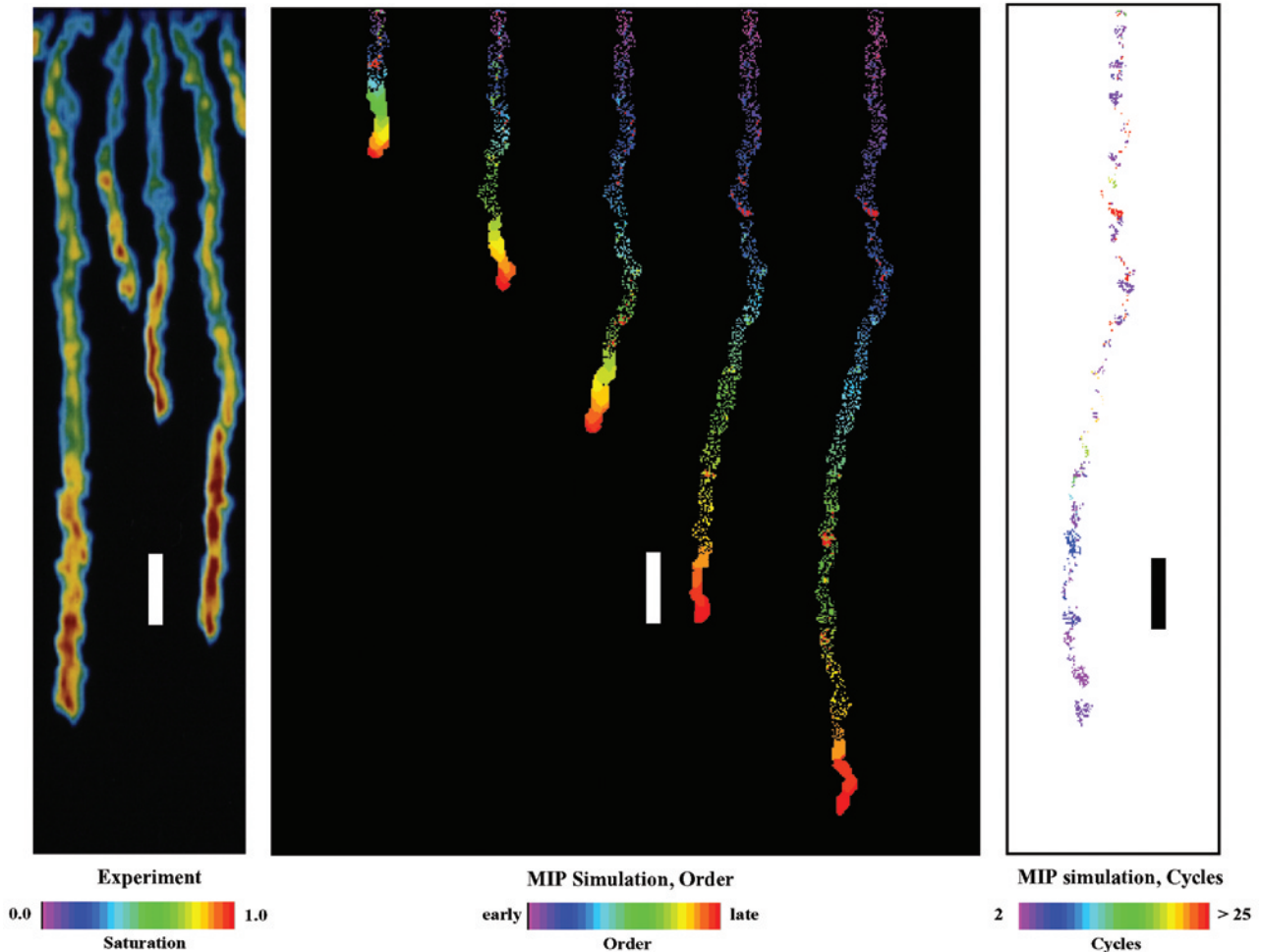
Figure 1. Gravity-driven wetting fingers in sand: (a) 15 cm wide by 60 cm tall portion of an experimental saturation field measured by *Glass et al.* [1989a] taken within the 20−30 sand directly below the restrictive 140−200 sand layer. (b) MIP growth order is shown in a sequence of images at the same scale as the experimental data in Figure 1a. Pulses (red zones) can be seen moving down the finger within the fragmented zone behind the finger tip. (c) MIP simulation cycle image shows pulsation to occur along the backbone of the fragmented zone behind the finger tip. Cycle values above 25 were due to artificial cyclic vibration and set to 25 in the figure. Blocks in each plot are given for scale and are 1 × 5 cm. For full detail, zoom in on the plates. Animation 1 shows the simulation.

wetting case in porous media, we then consider the recent experiments of *Glass et al.* [2000a] where buoyancy-driven migration of CO_2 in macro-heterogeneous sands showed not only pore scale fingering but fragmentation and pulsation at larger scales. Finally, for fractures, we consider the wetting invasion studied by *Nicholl et al.* [1993] where a single gravity-driven water finger is generated from a point source located at the top of a dry, vertical rough-walled fracture formed by two textured glass plates.

3.1. Gravity-Driven Wetting Fingers in Sand

[23] *Glass et al.* [1989a] developed and applied a light transmission technique to obtain water saturation fields during an unstable infiltration event within a fine (140−200 sieve fraction) over coarse (20−30 sieve fraction) layered sand system. Figure 1a shows a 15 cm wide by 60 cm tall subsection of one of these fields located within the bottom coarse layer where fingers occurred. While we do not have properties appropriate for the NP-MMIP model

application measured for this particular coarse sand, we have made such measurements on other narrow grain size distribution sands that support gravity-driven fingering.

[24] For our example simulation, we use the R_d distribution determined from drainage curves for a 12−20 Acu-sand as measured by *Glass et al.* [2000a]. Because spatial correlation within the coarse sand of the experiment was slight, we created a random, spatially uncorrelated 2D R_d field 15 cm wide by 60 cm tall with a grid spacing given by the sand's mean grain size of 0.1087 cm (i.e., 137 by 577 nodes). For either water or air invasion we assume contact angles of 0 and 180, respectively (i.e., no contact angle hysteresis), a density difference of 1 gm/cm^3, and a surface tension of 72 dynes/cm. We consider a diagonal network connectivity of 8 (up, down, left, right, and diagonals between) as has been shown to approximate 3D behavior in 2D networks. Water was supplied to 10 nodes (∼1 cm wide) in the middle of the top of the network to simulate an individual finger and invasion allowed to proceed.

[25] A sequence of invasion growth images from the simulation are shown in Figure 1b with color representing filling order in each. An animation of the simulation is shown in Animation 1. Qualitatively, we see a macroscopic saturated finger tip that drains a distance behind in both simulation and experiment. The saturated finger tip length, L_s, in the experiment was found to obey the relation

$$L_s = \frac{\psi_{we} - \psi_{ae}}{1 - R_f} \qquad (10)$$

where ψ_{we} is the water entry and ψ_{ae} the air entry values of the pressure and R_f is the ratio of the flux through the finger to the saturated conductivity of the medium. For very low flow rates as in our simulation ($R_f \sim 0$), (10) yields a value of $\sim$5 cm for the 12–20 Acu-sand (where $\psi_{we} \sim 5$ cm and $\psi_{ae} \sim 10$ cm [see *Glass et al.*, 2000a]), which matches that from our simulation ($\sim$5 cm). Finger width in the simulation is $\sim$1 cm and matches that found by *Glass et al.* [1989b] in an angular 14–20 sand at low flow rates ($\sim$1 cm) as well as earlier static simulations by *Glass and Yarrington* [1996]. We note that while details such as connectivity and the dimensionality of the network (2D versus 3D) will have a small influence on simulated finger width [see *Glass and Yarrington*, 1996], the size of the source at the top of the problem does not.

[26] Further consideration of the MIP growth sequence clearly shows the drainage zone behind the finger tip to fragment. Water pulses from the inlet, through the fragmented zone along a narrow "backbone" and on to the finger tip, causing the tip to advance and then stall as the pulse is spent. Analyzing the simulation to generate a cycle image that depicts the number of times a node fills and empties (Figure 1c), shows that some nodes along the backbone within the drained region cycle. To date, such pulsation behind finger tips has not been found experimentally for wetting gravity-driven fingers; however, it has for nonwetting such as in our next example problem. It is likely that this discrepancy is due to the action of film flow, as occurs with wetting fluids, or viscous forces, both of which have not been included in our current model.

3.2. Buoyancy-Driven Nonwetting Invasion in Heterogeneous Sands

[27] *Glass et al.* [2000a] presented experiments that considered nonwetting gravity/buoyant destabilized invasion (CO_2, TCE) in a water saturated, heterogeneous sand pack composed of three sands (12–20, 30–40, and 50–70 sieve fraction Acu-sands) arranged in a fashion analogous to fluvial cut and fill architecture. While subsequent analysis determined that viscous influences were nonnegligible in the TCE invasion experiments, the CO_2 injection conformed to the quasi-static assumption. Figure 2b shows the saturation field (26 cm wide, 55.5 cm tall) from the CO_2 experiment at the time just after the CO_2 had reached the top. An animation of the experimental images is shown in Animation 2. A cycle image was generated by comparing sequential images and noting whether a location had increased or decreased in saturation (Figure 2c). We see both pulsation at the small scale within fingers beyond capillary barriers as well as at the unit scale where "throbbing" is observed.

[28] Neglecting viscous forces, 3D network simulations for the CO_2 invasion using NP-MMIP modeled the evolu-

tion of the maximum extent of the invasion structure, its saturation, finger structure and maximum pool height behind capillary barriers, but of course, not the pulsation [*Glass et al.*, 2001]. For our example simulation where simultaneous wetting and nonwetting invasion is implemented, we consider a 2D network with an R_d field (Figure 2a) generated similarly to those of *Glass et al.* [2001]. R_d distributions measured for each of three sands (12–20, 30–40, and 50–70) were assigned to a unit structure created from digital images of the experimental pack (we refer the reader to details contained in that earlier paper). The grid spacing within the 26 cm wide by 55.5 cm tall domain was taken as the mean grain size of the 12–20 sand (0.1087 cm) yielding a 240 by 511 node problem and, once again, a diagonal connectivity of 8 was employed to simulate a 3D network in 2D. Fluid properties reflected the density difference between water and CO_2 of 0.994 gms/cm^3, interfacial tension of 71.4 dynes/cm and contact angles of 0 and 180 for water and CO_2 respectively (i.e., no contact angle hysteresis). CO_2 invaded from a small region corresponding to the septum through which gas entered in the experiment. At the top of the experiment, CO_2 was not allowed to leave the problem domain and thus pooled at the boundary. The simulation was terminated once the total volume of CO_2 injected into the problem was similar to that for the time period over which the cycle image presented in Plate 2c was built.

[29] An animation of the simulation is presented in Animation 3 and shows qualitatively similar phase growth, pulsation and unit scale throbbing as the experiment. Analysis of the simulation to yield a cycle image as was done with experimental data is shown in Figure 2d. Detailed comparison of the cycle images is made somewhat difficult due to both noise within the experimental data as well as light scattering that causes a cycling pore to influence the reading in other nearby pores, both of which cause a blurring in the experimental cycle image. However, in general, locations where pulsation occurs as well as where it does not (i.e., pool zones behind capillary barriers) are both reasonably well reproduced. We also find the minimum pool heights to be reasonably matched ($\sim$3 cm in both the simulation and the experiment, see top pool in Figures 2c and 2d). Finally, the range of cycles detected experimentally and in the simulation is comparable (see colors in Figures 2c and 2d). However, we do see the zone before the first capillary barrier to throb at a much higher rate in the simulation, while in the experiment, higher rates of pulsation are found directly below capillary barriers. In addition, the experiment shows roughly twice as many pulses to fill the pool before the final capillary barrier. It is likely that these specific discrepancies are due to local differences between the R fields especially at capillary barriers; additionally, we have not included the slight spatial correlation within the R field as likely present in the experiment, and the simulations are 2D rather than 3D. Finally, we note that within the free fingering zone beyond the final capillary barrier, multiple fingers form in the experiment but only a single finger of coursing CO_2 is simulated.
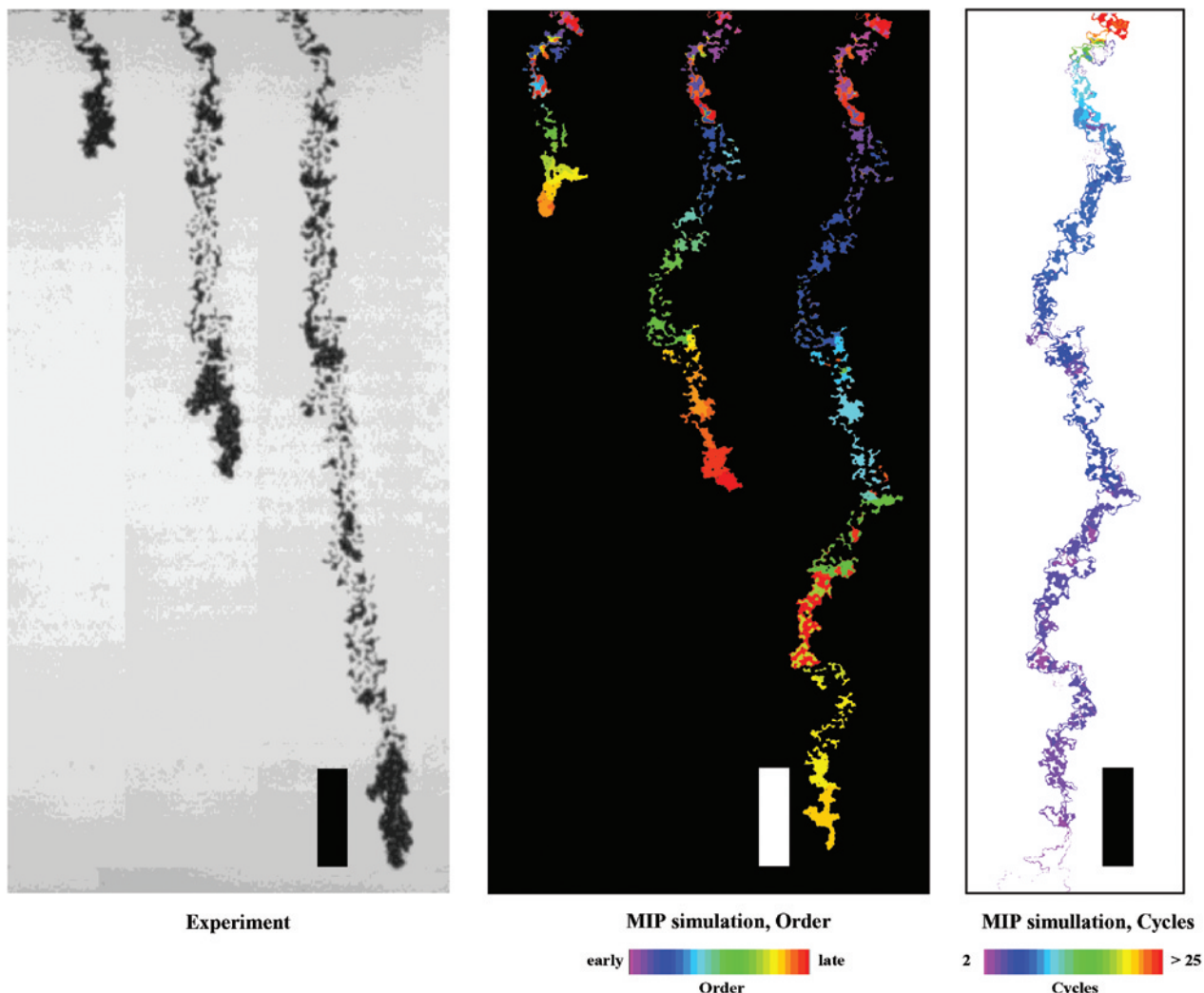
3.3. Gravity-Driven Wetting Fingers in Rough-Walled Fracture

[30] *Nicholl et al.* [1993] reported a series of experiments where single gravity-driven water fingers were generated
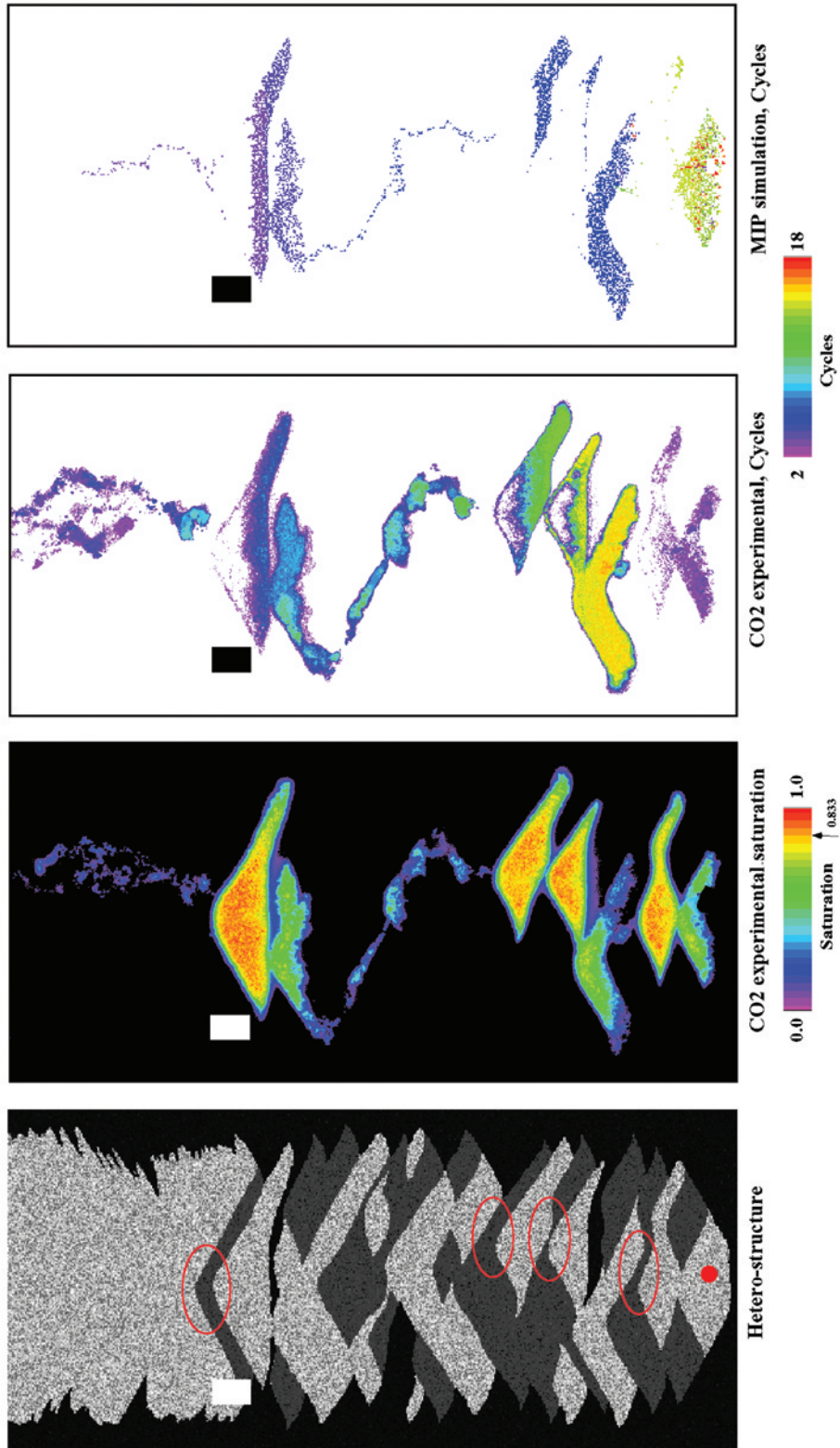
Figure 2. Buoyancy-driven nonwetting invasion in heterogeneous sand: (a) Simulated R field derived from experimental heterogeneous sand structure (26 cm wide, 55.5 cm tall) of *Glass et al.* [2000a, 2001] showing the fine sand (dark, 50−70), medium sand (intermediate, 30−40), and coarse sand (light, 12−20) units. Capillary barriers are circled and the CO_2 injection port near the bottom is shown in red. (b) Saturation image just after CO_2 reached the top of the initially water filled chamber. (c) Experimental cycle image showing pulsation within fingers and unit scale throbbing. (d) MIP simulation cycle image. Cycle values above 18 were due to artificial cyclic vibration and set to 18 in the figure. Blocks in each plot are given for scale and are 2 × 3 cm. For full detail, zoom in on the plates. Animations 2 and 3 show the experimental images and simulation, respectively.

Figure 3.   Gravity-driven wetting fingers in rough-walled fractures: (a) Sequence of 26.5 cm tall image portions show a gravity-driven finger (water, dark) generated from a point source at the top of an initially dry, transparent, water-wettable, rough-walled fracture composed of two pieces of textured glass (from experiments of *Nicholl et al.* [1993]). (b) MIP growth order is shown in a sequence of images at the same scale as the experimental data in Figure 3a. Pulses (red zones) can be seen moving down the finger within the fragmented zone behind the finger tip. (c) MIP simulation cycle image shows pulsation to occur throughout the fragmented zone behind the finger tip. White zones surrounded by color are water filled and do not cycle. Cycle values above 25 were due to artificial cyclic vibration and set to 25 in the figure. Blocks in each plot are given for scale and are 1 × 3 cm. For full detail, zoom in on the plates. Animations 4 and 5 show the experimental images and simulation, respectively.

within an initially dry, inclined, transparent, analogue rough-walled fracture from a point source at its top. In the experiments, wetted structure was captured within a 13 by 28 cm portion of the 15 by 30 cm fracture (a cm wide gasket around the fracture edges blocked the view) in a series of digital images (256 gray levels, 512 by 512 pixels). Figure 3a shows a sequence of images for an experiment at their lowest flow rate (0.026 mL/min) in a vertical fracture (experiment F80). An animation of the experimental images is shown in Animation 4. Unfortunately, the noise level in these early experimental images was too high to obtain clear cycle images.

[31] For our example simulation, we use the aperture field of a similar fracture measured with a light transmission technique at 0.15 mm resolution by *Detwiler et al.*

[1999]. Analysis of the internal 12 cm by 26.46 cm portion of the 15 cm by 30 cm aperture field yields a mean of 0.225 mm, coefficient of variation of 0.274 and spatial correlation length of ∼0.75 mm. We simulated water invasion into this 800 by 1764 node aperture field from a 50 node wide (0.75 cm) zone at the top of the vertical fracture using fluid properties for the air and water as mentioned above in our first example and contact angles of 30 degrees for wetting and 150 degrees for drainage representative of experimental measurements (i.e., no contact angle hysteresis). In the fracture formulation, a connectivity of 4 (up, down, right, left) is used and phase trapping is implemented.

[32] Animations of both the experiment and the simulation show the finger tip to move downward with a stop and

go dynamic. The finger first overruns supply, fragments behind, and then stalls. This is then followed by the arrival of the next pulse transmitted through the fragmented zone, after which the process is repeated. A sequence of images from the simulation is shown in Figure 3b. Once again, the color in the growth images represents filling order and clearly shows the pulsing of water from the inlet, through the fragmented zone, and on to the finger tip. An animation of the simulation is presented in Animation 5. The cycle image for the simulation (Figure 3c) shows that the pulses traveling within the fragmented zone swell the clusters slightly when they touch (colored rim around white "stable" clusters within the finger) and then shrink them back just as they become disconnected from the downward moving pulse. This small scale swelling and shrinkage appears realistic in magnified portions of animations.

[33] In comparison to the experiment, the structure at the finger tip, the fragmentation zone behind, and the coursing of the fluid down to replenish the finger tip, all match reasonably well. Average finger widths in the simulation ($\sim$0.8 cm) are slightly less than those in the experiment ($\sim$1 cm) and conform to earlier static MIP simulations by *Glass* [1993] that used a rudimentary algorithm for in-plane interfacial curvature. We note that the finger tip is in general greater than 10 correlation lengths in width and maintains a macroscopic, "saturated" tip that drains a distance behind. This finger tip in the experiment and simulation fluctuates in length about mean values of $\sim$3 and $\sim$2 cm, respectively. Since we have not included contact angle hysteresis in our simulations, the r_2 curvature alone causes this hysteretic behavior. Without it, the finger tip and fragmented zone structure would be defined by the correlation length of the aperture field. Additionally, one would find pulsation at the microscale where single grid-block packets of fluid are passed along the structure in time, a phenomenon we have not witnessed in experiments conducted to date. While unwarranted at this time, we note that closer matches between simulation and experiment for finger width and finger tip length can be had by slight modifications of the aperture field and its λ, the way the in-plane curvature is calculated (weighting for γ), the wetting contact angle (α) and by including contact angle hysteresis.

4. Discussion

[34] Our mechanistic MIP based model includes gravity, the influence of local geometry of the phase-phase interface, and the simultaneous invasion and reinvasion of wetting and nonwetting fluids. Including all of these components allows us to model many qualitative and quantitative aspects of gravity/buoyant destabilized unsaturated/two-phase flows. In particular, in both porous media and fractures, we simulate the macroscopic (wetting) vs. pore-scale (nonwetting) fingers, drainage behind finger tips, as well as fragmentation and pulsation under appropriate conditions. We also find reasonable quantitative concurrence with experiments for measures such as finger width, saturated finger tip lengths and maximum and minimum pool heights in macro-heterogeneous porous media. Such agreement is the required first step in the development of a complete mechanistic model for such unstable flows.

[35] However, we find two significant discrepancies with experiment across the example problems. First, for gravity-driven wetting fingers in sand, our simulations show the wetting phase behind the fingertip to be become fully fragmented with a narrow backbone that quasiperiodically connects the source to the growing finger-tip. The structure and behavior of the backbone is similar to that which is found for gravity-driven nonwetting fingers but we are unaware of experimental evidence demonstrating wetting phase fragmentation/pulsation to occur under these circumstances. For situations where conductive liquid films are not maintained on the surfaces of grains, we would expect fragmentation/pulsation such as seen in fracture experiments and simulations. We believe this behavior should be considered further both through additional extensions of the MIP model (i.e., include first order viscous effects such as conduction within liquid films) and experimentally (i.e., explore situations where liquid films are, and are not, maintained on drainage).

[36] Second, we do not find multiple pathways to often form in our simulations. This is because the filling and vacating pressures for pores across the field are almost always distinguishable by the algorithm. However, in reality, we might expect that the flow would not be able to make such distinctions all the time due to such mechanisms as dynamic contact angles or variable inertial forces within pores during a Haines jump. At places where the choice between two nodes falls below the level of discrimination, the pathway is likely to switch. Such randomness can be included directly within the model and will lead to behavior similar to that seen experimentally. As an example, we mention that in fracture simulations, the calculation of in-plane curvature sometimes causes individual apertures to be indistinguishable via computer round-off and thus a new pathway is occasionally formed.

[37] So far, we have considered only a few example situations in porous media and fractures where fingering and associated phenomena occur. However, pulsation phenomona have been documented in many other situations as well. Under conditions of constant inflow, oscillation in outflow has been found in coarse porous media [*Prazak et al.*, 1992] and in fracture-matrix networks [*Glass et al.*, 2002]. The combination of gravity-driven fingering and pulsation in fracture-matrix networks has also been found to create new flow paths in time and cause the sporadic switching of flow from one path to another [*Glass et al.*, 2002]. Additionally, situations have been documented where pulsation occurs in horizontal fractures such as during the concurrent gas-liquid flow in a horizontal fracture [*Persoff and Pruess*, 1995] or during slow nonwetting displacement [*Amundsen et al.*, 1999]. Some of these situations are directly assessable to analysis with the current MIP model while others will require further augmentation along the lines pointed out above.

5. Concluding Remarks

[38] Full understanding of fingering, nonmonotonicity, fragmentation and pulsation is far from complete. All these phenomena are emergent, that is, they arise from the underlying physics to yield spatial and temporal behavior of their own. Length scales emerge that are predictable from simple scale analyses for pore scale (nonwetting) to macroscopic (wetting) finger width, finger tip length, pool heights in heterogeneous media, as well as for the distribution of blob sizes within fragmented zones. Temporal behavior emerges

with pulsation that is "periodic" to "quasiperiodic", "erratic", or "chaotic" in time. For all, we find history to play a role and impart a certain degree of persistence in structure or pattern while fluctuations create multiple pathways, often only one of which conducts at any particular time. It is also possible that this phenomenon may result in behavior at larger scales rather than simply "averaging out".

[39] In this paper we have introduced a mechanistic model that includes gravity, the influence of local geometry of the phase-phase interface, and the simultaneous invasion and reinvasion of wetting and nonwetting fluids. We have shown that it conforms to many aspects of published experiments for three very different situations. For a range of reality, the model is sufficiently accurate to consider full parametric studies where fingering, fragmentation and pulsation are studied as a function of system parameters. However, through our experimental comparisons, we have also identified several processes that must be further incorporated within the MIP model to treat the full realm of possibility. The further incorporation of film flow, viscous and local inertial forces, at least, must be considered. To guide this further development, additional experiments will be required where accurate measurements are made of pulsation dynamics, fragmented blob structure, and multiple pathway formation, all as a function of material properties and boundary/initial conditions.

References

Amundsen, H., G. Wagner, U. Oxaal, P. Meakin, J. Feder, and T. Jossang, Slow two-phase flow in artificial fractures: Experiments and simulations, *Water Resour. Res.*, 35(9), 619–2626, 1999.

Auradou, H., K. J. Maloy, J. Schmittbuhl, A. Hansen, and D. Bideau, Competition between correlated buoyancy and uncorrelated capillary effects during drainage, *Phys. Rev. E*, 60, 7224–7234, 1999.

Blunt, M. J., and H. Scher, Pore-level modeling of wetting, *Phys. Rev. E*, 52, 6387–6403, 1995.

Detwiler, R. L., S. E. Pringle, and R. J. Glass, Measurement of fracture aperture fields using transmitted light: An evaluation of measurement errors and their influence on simulations of flow and transport through a single fracture, *Water Resour. Res.*, 35(9), 2605–2617, 1999.

Ewing, R. P., and B. Berkowitz, A generalized growth model for simulating initial migration of dense non-aqueous phase liquids, *Water Resour. Res.*, 34(4), 611–622, 1998.

Glass, R. J., Modeling gravity-driven fingering in rough-walled fractures using modified percolation theory, in *High Level Radioactive Waste Management, Proceedings of the Fourth Annual International Conference*, pp. 2042–2053, Am. Nuclear Soc., New York, 1993.

Glass, R. J., and M. J. Nicholl, Physics of gravity-driven fingering of immiscible fluids within porous media: An overview of current understanding and selected complicating factors, *Geoderma*, 70(2–4), 133–163, 1996.

Glass, R. J., and L. Yarrington, Analysis of wetting front instability using modified invasion percolation theory, *Eos Trans. AGU*, 70, 1117, 1989.

Glass, R. J., and L. Yarrington, Simulation of gravity fingering in porous media using a modified invasion percolation model, *Geoderma*, 70(2–4), 231–252, 1996.

Glass, R. J., T. S. Steenhuis, and J.-Y. Parlange, Mechanism for finger persistence in homogeneous unsaturated porous media: Theory and verification, *Soil Sci.*, 148, 60–70, 1989a.

Glass, R. J., T. S. Steenhuis, and J.-Y. Parlange, Wetting front instability, 2, Experimental determination of relationships between system parameters and two-dimensional unstable flow field behavior in initially dry porous media, *Water Resour. Res.*, 25, 1195–1207, 1989b.

Glass, R. J., E. K. Webb, and S. H. Conrad, An upscaled buoyant invasion percolation model for use in approaches to delineate subsurface DNAPL location, *AIChE Symp. Ser.*, 306(91), 23–29, 1995.

Glass, R. J., M. J. Nicholl, and L. Yarrington, A modified invasion percolation model for low-capillary number immiscible displacements in horizontal rough-walled fractures: Influence of local in-plane curvature, *Water Resour. Res.*, 34(12), 3215–3234, 1998. (Correction, *Water Resour. Res., 36*(7), 1991, 2000.)

Glass, R. J., S. H. Conrad, and W. Peplinski, Gravity destabilized nonwetting phase invasion in macroheterogeneous porous media: Experimental observations of invasion dynamics and scale analysis, *Water Resour. Res.*, 36(11), 3121–3137, 2000a.

Glass, R. J., M. J. Nicholl, and L. Yarrington, Correction to "A modified invasion percolation model for low-capillary number immiscible displacements in horizontal rough-walled fractures: Influence of local in-plane curvature" by Robert J. Glass, Michael J. Nicholl, and Lane Yarrington, *Water Resources Research*, 36(7), 1991, 2000b.

Glass, R. J., S. H. Conrad, and L. Yarrington, Gravity destabilized nonwetting phase invasion in macroheterogeneous porous media: Near pore scale macro modified invasion percolation model, *Water Resour. Res.*, 37(5), 1197–1207, 2001.

Glass, R. J., S. E. Pringle, M. J. Nicholl, and T. R. Wood, Unsaturated flow through a fracture-matrix-network: Dynamic pathways in mesoscale laboratory experiments, *Water Resour. Res.*, 38(12), 1281, doi:10.1029/2001WR001002, 2002.

Hill, D. E., and J.-Y. Parlange, Wetting front instability in layered soils, *Soil Sci. Soc. Am. Proc.*, 36, 697–702, 1972.

Hughes, R. G., and M. J. Blunt, Network modeling of multiphase flow in fractures, *Adv. Water Resour.*, 24(3–4), 409–421, 2001.

Ioannidis, M. A., I. Chatzis, and F. A. L. Dullien, Macroscopic percolation model of immiscible displacement: Effects of buoyancy and spatial structure, *Water Resour. Res.*, 32(11), 3297–3310, 1996.

Kueper, B. H., and D. B. McWhorter, The use of macroscopic percolation theory to construct large-scale capillary pressure curves, *Water Resour. Res.*, 28(9), 2425–2436, 1992.

Meakin, P., A. Birovljev, V. Frette, J. Feder, and T. Jossang, Gradient stabilized and destabilized invasion percolation, *Physica A*, 191, 227–239, 1992.

Meakin, P., G. Wagner, J. Feder, and T. Jossang, Simulations of migration, fragmentation, and coalescence of nonwetting fluids in porous-media, *Physica A*, 200, 241–249, 1993.

Nicholl, M. J., R. J. Glass, and H. A. Nguyen, Small-scale behavior of single fingers in an initially dry fracture, in *High Level Radioactive Waste Management, Proceedings of the Fourth Annual International Conference*, pp. 2023–2032, Am. Nuclear Soc., New York, 1993.

Persoff, P., and K. Pruess, Two-phase flow visualization and relative permeability measurement in rough-walled fractures, *Water Resour. Res.*, 31(5), 1175–1186, 1995.

Prat, M., Percolation model of drying under isothermal conditions in porous media, *Int. Multiphase Flow, J.*, 19(4), 691–704, 1993.

Prazak, J., F. Kublik, I. Tywoniak, and C. Zarcone, Oscillation phenomena in gravity-driven drainage in coarse porous media, *Water Resour. Res.*, 28(7), 1849–1856, 1992.

Selker, J. S., P. Leclerq, J.-Y. Parlange, and T. S. Steenhuis, Fingered flow in two dimensions, 1, Measurements of matric potential, *Water Resour. Res.*, 28(9), 2513–2521, 1992.

Schwille, F., *Dense Chlorinated Solvents in Porous and Fractured Media*, A.F. Lewis, Boca Raton, Fla., 1988.

Su, G. W., J. T. Geller, K. Pruess, and F. Wen, Experimental studies of water seepage and intermittent flow in unsaturated, rough-walled fractures, *Water Resour. Res.*, 35(4), 1019–1037, 1999.

Su, G. W., J. T. Geller, K. Pruess, and J. R. Hunt, Solute transport along preferential flow paths in unsaturated fractures, *Water Resour. Res.*, 37(10), 2481–2491, 2001.

Wagner, G., P. Meakin, J. Feder, and T. Jossang, Buoyancy-driven invasion percolation with migration and fragmentation, *Physica A*, 245, 217–230, 1997.

Wilkinson, D., and J. F. Willemsen, Invasion percolation: A new form of percolation theory, *J. Phys. A Math. Gen.*, 16, 3365–3376, 1983.

Xu, B., Y. C. Yortsos, and D. Salin, Invasion percolation with viscous forces, *Phys. Rev. E*, 57(1), 739–751, 1998.

————————————

R. J. Glass and L. Yarrington, Flow Visualization and Processes Laboratory, Sandia National Laboratories, Albuquerque, NM 87185-0735, USA. (rjglass@sandia.gov)